Optical Development in the Zebrafish Eye Lens

Kehao Wang[1], Irene Vorontsova[2,3], Masato Hoshino[4], Kentaro Uesugi[4], Naoto Yagi[4], James E. Hall[2], Thomas F. Schilling[3], Barbara K. Pierscionek[1]*

1. School of Science and Technology, Nottingham Trent University, Nottingham, NG11 8NS, UK
2. Department of Physiology and Biophysics, University of California Irvine, Irvine, CA 92697, USA
3. Department of Developmental and Cell Biology, University of California Irvine, Irvine, CA 92697, USA
4. Japan Synchrotron Radiation Research Institute (Spring-8), 1-1-1, Kouto, Sayo-cho, Sayo-gun, Hyogo 679-5198, Japan

Correspondence email: barbara.pierscionek@ntu.ac.uk

Nonstandard Abbreviations:

GRIN: Gradient Refractive Index

ARVO: Association for Research in Vision and Ophthalmology

IACUC: Institutional Animal Care and Use Committee

Abstract

The optics of the eye is key to a functioning visual system. The exact nature of the correlation between ocular optics and eye development is not known because of the paucity of knowledge about the growth of a key optical element, the eye lens. The sophisticated optics of the lens and its gradient of refractive index provide the superior optical quality that the eye needs and which, it is thought, has a major influence on the development of proper visual function. The nature of a gradient refractive index lens, however, renders accurate measurements of its development difficult to make and has been the reason why the influence of lens growth on visual function remain largely unknown. Novel techniques have made it possible to investigate growth of the eye lens in the zebrafish. This study shows measurements using X-ray Talbot interferometry of three-dimensional gradient index profiles in eye lenses of zebrafish from late larval to adult stages. The zebrafish lens shows evidence of a gradient of refractive index from the earliest stages measured and its growth suggests an apparent coincidence between periods of rapid increase in refractive index in the lens nucleus and increased expression of a particular crystallin protein group.

Keywords:

zebrafish, eye lens, vision, ocular development.

Introduction

The eye lens is one of two optical elements that focus an image on the retina. Lens development begins in early embryonic life but is difficult to observe in mammals and most vertebrate species [1]. The lens is a complex optical system that provides a high level of image quality and a structure/function relationship that maintains transparency for a greater part of the lifespan. It is contained within a semi-elastic capsule and grows by laying down concentric layers of fibre cells over existing tissue with no concomitant cell loss. Epithelial cells proliferate, differentiate and elongate into lens fibre cells at the lens equator [2]. Fibre cells contain very high concentrations of structural proteins, collectively called crystallins, and these concentrations vary across the lens from periphery to centre to create a gradient of protein concentration [3]. Protein concentration is linearly related to refractive index [4], and the distribution of the crystallin proteins across the lens creates a gradient refractive index or GRIN lens (reviewed in [5]). Such a lens has the superior optical quality required for vision. What causes the proteins to be distributed in such a way as to create the requisite GRIN profile for the particular eye of any given species is not known because of the paucity of studies on the development of the GRIN from very early stages of growth.

The zebrafish provides a number of advantages over mammalian models for studying the development of GRIN lens: embryonic development is external and rapid [1], an optokinetic response is evident at three days post-fertilization [6]; and both the lens and whole animal grow throughout life, allowing assessment of effects of size and age on optics. In addition, whilst in the mammalian eye the cornea contributes the greater amount of optical refraction, in aquatic species the lens is the major optical component on which the eye depends for maintenance of image quality [7].

Materials and Methods

Sample preparation

The animal protocols used in this study adhere to the ARVO (Association for Research in Vision and Ophthalmology) Statement for the Use of Animals in Ophthalmic and Vision Research and have been approved by the IACUU (Institutional Animal Care and Use Committee) of University of California, Irvine. Zebrafish (AB strain) were raised and maintained under standard laboratory conditions [8]. Larval or adult zebrafish were anesthetized in tricaine (MS-222; Sigma, St. Louis, MO). Eyes were dissected from animals younger than a month, and lenses were dissected [9] from animals older than a month. During dissection and for transport of tissues to the measurement facility the samples were kept in BioWhittakerTM DMEM with 25 mM Hepes and 4.5 g/l glucose, without L-Glutamine (Lonza, Morristown, NJ) supplemented with 1ug/ml

of penicillin/streptomycin at room temperature. For *in vivo* lens transparency assessment, a fibre optic light source (Schott KL 1500; Schott AG, Mainz, Germany) was used for oblique illumination from two sides to visualise opacities. Transparency of dissected lenses was visualised with an Olympus SZX12 microscope using an Olympus DP70 digital camera with an Olympus DP Controller (2.1.1.183) (Tokyo, Japan) under darkfield and brightfield illumination. Prior to data acquisition, lenses in DMEM that turned yellow were discarded, as this indicated lens damage. Lenses were transported in DMEM in Eppendorf tubes at room temperature to the SPring-8 synchrotron and were measured within a week of dissection. Measurements were conducted once a year and data collected in three consecutive years were combined for this study.

Lens immunohistochemistry

Dissected adult lenses were fixed and cryo-sectioned as previously described [10]. Lens sections were labelled with the plasma membranes marker wheat germ agglutinin AlexaFluor 594 (1:50; Life Technologies, Grand Island, NY, USA) and DAPI (1:1000) overnight at 4˚C. Images were acquired with a confocal microscope and imaging software (Nikon Eclipse Ti-E with NIS-Elements AR; Nikon Corp., Tokyo, Japan). Images were viewed and compiled with ImageJ, version 1.51n (http://imagej.nih.gov/ij/; provided in the public domain by the National Institutes of Health, Bethesda, MD, USA) and a raster graphics editor (Adobe Photoshop CS5, version 12.0; Adobe Systems, San Jose, CA, USA).

X-ray Talbot interferometry

The three-dimensional GRIN distribution of each sample was measured using a phase contrast imaging modality: X-ray Talbot interferometry [11, 12, 13]. Experiments were conducted at the bending magnet beamline BL20B2 at SPring-8 using monochromatic X-ray beam, fine-tuned to 25 keV. The X-ray beam passes through a Si(111) double-crystal monochromator and two transmission gratings: a tantalum phase grating (G1) and a gold absorption grating (G2) with pattern thicknesses of 2.1 μm and 16.6 μm, respectively. Both gratings have a pitch of 10 μm and a pattern size area of 25×25 mm^2. Grating G2 has an inclination angle of 45 degrees. Moiré fringe patterns generated by X-ray beam passing through the sample and two gratings were detected by a scientific CMOS detector (ORCA Flash 4.0. Hamamatsu Photonics). G2 was shifted using a 5-step ‘on-the-fly’ fringe-scan method with a Piezo stage for phase retrieval. Different phase images obtained from the scan were integrated to get the phase shift image. Five different solutions of known density [11, 14] were used to calibrate the phase shifts by comparing experimentally obtained values to theoretically derived values per pixel. Linear relationships were found over the range of tested concentrations. Using equations described by Hoshino et al. [11], X-ray refractive index difference was determined from the phase shifts per pixel and was further used to calculate the protein concentration from

which refractive index was calculated. For each lens, the total number of scans was 900 with a time of measurement of around 50 minutes.

Zebrafish staging

Due to the asynchronous growth of zebrafish, which depends on a multitude of factors such as population density, tank size, food availability, temperature and water quality, age is not a good indicator of post-embryonic zebrafish development. Hence, post-embryonic animals (after hatching of the chorion, which occurs at 48-72 hours post fertilization [15]) were staged by their standard length (snout to start of tail) [16]. Since standard length could not be correlated with specific pair of lenses due to practicality of pooling samples from different animals, equatorial lens diameters were used as a measure of developmental stage. Zebrafish lenses are not precisely spherical, and this asymmetry varies with age. The lens anterior-posterior dimension is slightly larger at larval and early juvenile stages and the equatorial diameter (perpendicular to the optical axis) is larger in older juvenile and adult stages (Figure 1). To identify the equatorial diameter, 3D images of lenses were analysed in perpendicular planes looking for asymmetries in localization of the lens nucleus at younger stages [9, 10] as a landmark for orientation in excised lenses and/or anatomy of the surrounding eye tissues. A precise measurement was acquired using SolidWorks (ver. 2017, Waltham, Massachusetts, USA) by fitting a circle to the contour plot in equatorial plane of each lens.

GRIN analysis

Mathematical computational software MatLab (ver. 2018a, Natick, Massachusetts, USA) was used to a) process raw refractive index values in the three-dimensional spatial domain; b) generate two-dimensional iso-indicial index contours and three-dimensional meshed index profiles in the equatorial plane of each lens and c) calculate parameters describing shapes of refractive index profile of each lens. Parameters used to describe varying shapes and magnitudes of the GRIN profiles along the optical axis of each lens at different ages include: the maximum index value at the peak of each index profile, the steepness of the peripheral part of each profile and the width of the central plateau region. The steepness of the peripheral region of each index profile was obtained by fitting the normalised index profile of each lens to an exponential power model [17]:

$$\mathrm{n(r)} = n_c + (n_s - n_c)r^g \quad (1)$$

where n is the refractive index, n_c is the refractive index at lens centre, n_s is the refractive index at lens surface, r is the normalised distance from the lens centre, g is the power exponent depicting the steepness of the index profile. A steeper profile is normally fitted to a higher g value [17]. An example of the original GRIN profile of a 157-day-old lens is shown in Figure 2a and its normalised profile fitted to the exponential

power model is given in Figure 2b. The central plateau region of the index profile was determined from the gradient of the original GRIN profile, selecting the region for which the gradient is within the range of -0.3mm^{-1} to 0.3mm^{-1}. An example of how the plateau region of the GRIN profile was determined for a 157 day old lens is shown in Figures 2c-e. The resolution of the refractive index measurement is 15.5 μm. At any given point, it is linearly related to the local protein concentration as described by the Gladstone-Dale formula [4]:

$$\mathrm{n} = n_s + \left(\frac{dn}{dC}\right) C \quad (2)$$

where n is the measured refractive index of each lens at various points, n_s=1.333 is the refractive index of the solvent (water), dn/dC=0.19ml/g [5] is the specific refractive increment of the crystallin proteins, C is the protein concentration of a local cubic volume of 15.5μm^3. This calculation can be used to obtain total protein content in any given lens.

Results

Development of GRIN in zebrafish lenses

We measured GRIN throughout zebrafish development to study effects of age versus lens size on its optical properties. Since lens diameter and zebrafish standard length are linearly related [10,18] we used lens diameter as an indicator of developmental stage. Growth in either parameter (Figure 3a-b) was fitted to an exponential growth model, which shows an initial rapid increase and gradual decrease with age, plateauing after 471 dpf. We observed a range of lens diameters and standard lengths in some cohorts of fish of the same age, highlighting the growth variability.

Measurements of refractive index distribution and two-dimensional refractive index contours in the optical axis plane were used to generate three-dimensional mesh plots for selected lenses with diameters ranging from 160 to 790 μm (Figure 4). Lens diameters were measured using the second outermost (Figure 4a) or the outermost (Figure 4b-h) contour. Lenses at all stages exhibit smooth and symmetrical three-dimensional GRIN profiles, with the magnitude of refractive index increasing progressively from the lens surface to the lens centre (Figure 4a-h) where it plateaus. The extent of this plateau increases with lens size and age (Figure 4d-h). The minimum index value found at the lens surface remains essentially unchanged across different ages, but the peak index value at the lens centre increases with age from approximately 1.43-1.44 for small lenses of 160 μm diameter (Figure 4a) to around 1.58 when the diameter reaches 540 μm (Figure 4e). The peak index value at the lens centre remains at this maximum value for lens diameters greater than

540 μm (Figure 4e-h).

Measurements of two-dimensional refractive index contours in the equatorial plane and three-dimensional mesh plots of GRIN distribution are shown for selected lenses with diameters ranging from 160 to 790 μm (Figure 4). Lens diameters were measured using the second outermost (Figure 4a) or the outermost (Figure 4b-h) contour. All refractive index contours are approximately circular (Figure 4); the youngest lens deviates slightly from this because it was measured in an intact eye (Figure 4a). Both the lens diameter and the size of its inner index plateau region increase with age (Figure 4a-h). Lenses at all stages exhibit smooth and symmetrical three-dimensional GRIN profiles, with the magnitude of refractive index increasing progressively from the lens surface to the lens centre (Figure 4a-h) where it plateaus. The extent of this plateau increases with lens size and age (Figure 4d-h). The minimum index value found at the lens surface remains essentially unchanged across different ages, but the peak index value at the lens centre increases with age from approximately 1.43-1.44 for small lenses of 160 μm diameter (Figure 4a) to around 1.58 when the diameter reaches 540 μm (Figure 4e). The peak index value at the lens centre remains at this maximum value for lens diameters greater than 540 μm (Figure 4e-h).

Maturation of shaping components of the GRIN profile

To quantify how the GRIN profile changes with growth and ageing, an exponential power model (Equation 1) was fitted to GRIN profiles along the central lens optical axis (Figure 5a). The slope of the GRIN profile becomes steeper (the power exponent g increases) with development (Figure 5). The smallest, youngest lens at 140 μm diameter (15 dpf), has a GRIN profile that is approximately linear (Figure 5b). As the lens diameter grows and the power exponent g increases to around 2, the GRIN profile approaches a parabolic form. With the steepening of the GRIN profile in larger and older lenses, the exponent g increases further, rising above 3.0 (Figure 5b).

The maximum refractive index increases rapidly in smaller lenses and the rate of increase slows down at older stages (Figure 6a). The power exponent g increases sigmoidally with lens diameter: rapid growth occurring when the lens diameter is between 250-450 μm and reaching a maximum value of around 3-3.5 as the lens diameter increases beyond 500 μm (Figure 6b). In contrast to the growth related trends in maximum refractive index and slope of GRIN profile, the initial increases in net protein weight and central plateau size are slow in lenses of diameters less than 300 μm and become more rapid in larger lenses (Figures 6c, d).

Effects of age and size on lens optics

The maximum refractive index appeared to be reached at 120 dpf with no further increase (Figure 6e). This fit is similar to that seen plotted as a function of lens diameter (Figure 6a). We therefore analysed maximum refractive index as a function of age and size. The power exponent, g, demonstrates a similar trend with age to that seen for maximum refractive index (Figure 6f). There is considerable variability in g value within age cohorts. The GRIN profiles from eight age groups (15, 32, 63, 66, 119, 472, 648, 880 dpf) are shown in Figure 7.The greatest spread of points occurs in samples aged 63-66 dpf, with a noticeable difference in the GRIN profile over this short time (Figure 7c, d), and this would account for the spread of values of exponent g in Figure 6f. Variability reflects the range of standard lengths from ~8-15 mm (Figure 3a). The profiles within all sets are very similar and this highlights the fact that even though the g exponent, which represents the slope of the GRIN profile, varies with age, there is very little divergence of the GRIN profile within a given age cohort. A comparison across cohorts emphasises that the GRIN profile changes systematically with age.

Discussion

The refractive index of the eye lens is critical for optical quality in the visual system. Measurement of the GRIN requires an intact lens, ideally within its natural environment in the eye, and non-invasive techniques that can determine the refractive index in any plane [5]. Here we use X-ray phase contrast tomography with a Talbot grating interferometer to measure the spatial profile of the refractive index in the zebrafish lens.

Our principle findings include: 1) a progressive increase in the slope of the GRIN with age, 2) attainment of a large maximum index of refraction, and 3) an increase in the size of the plateau region of index of refraction profile. Such developmental data have not previously been available for any species over such a large fraction of lifespan. This detailed optical analysis together with previous characterization of the centralization of the lens nucleus from anterior to central in the optical axis [10] as well as the changing geometry of the zebrafish eye throughout development [19,20], adds valuable insights that will lead to a model of how the zebrafish eye develops at different stages.

X-ray Talbot interferometry can provide the requisite image contrast for biological specimens [14] and reveal density differences at a resolution of 5-50μm [11]. The technique has been able to detect small fluctuations and kinks in the GRIN profile from several terrestrial species including human, porcine and murine lenses [11,21] and yet appear to be absent in the zebrafish lens (Figure 4). Such discontinuities most likely result from structural irregularities [11,21]. Kröger et al. [22] have noted ‘depressions’ in the outer part of GRIN profiles of the African Cichlid fish. Whether or not these are of similar nature to the

discontinuities seen in terrestrial species is not known. Zebrafish lenses have completely smooth GRIN profiles at all measured developmental stages (Figure 4). Subtle fluctuations in GRIN profile of eye lenses have provided an explanation of the optical zones of discontinuity [17], seen in living human eye [23]. These have been linked to age [23] and postulated to be linked to a stepwise growth pattern [5]. The absence of discontinuities in the GRIN profiles in the zebrafish lens could reflect their small size, such that any fluctuations are too minute to detect. The African cichlid fish lenses measured by Kröger et al. [22] were considerably larger, at around 2.4-2.6 mm diameter, than the largest zebrafish lens in this study, of ~800 μm. Alternatively, the zebrafish lens may lack the periodic growth spurts found in terrestrial species, if indeed these are the cause of discontinuities.

The present study is the first to describe the development of the refractive index in the zebrafish lens. The only other study of GRIN development was on foetal bovine lenses, which showed that the GRIN starts to form at around 4-5 months gestation, prior to which it has no particular form [24]. Although light was suggested as an influence on the magnitude of refractive index in fish lenses [25], it is not known what factors trigger the development of lens optics. A GRIN lens reduces optical aberrations [26, 27, 28] and provides the eye with high image quality.

Shape and magnitude of refractive index vary among eye lenses of different species, and this is related to species-specific visual requirements [5]. Visually-guided behaviour appears shortly after hatching in clownfish [29] and visually evoked body twitch responses in zebrafish are detected as early as 68-79 hours post-fertilization [6]. After 5 dpf, zebrafish rely on vision for survival, hunting and evading predators.

Refractive index profiles of aquatic lenses have been fitted to a number of functions including: higher-order polynomials [30, 31], parabolic [22, 32] and elliptical profiles [33]. Exponential power models used to fit the GRIN profiles of zebrafish lenses in the present study have previously been applied to porcine [34] and human lenses [17]. This power model has the advantage of containing fewer coefficients and provides an optimal fit to the refractive index profile in porcine [34] and human lenses [17]. The steepness of the GRIN profile in zebrafish lenses changes greatly with development (Figure 6b and 6f) as evidenced by the range of the power exponent g across the range of samples measured (Figure 5b). The steepening of GRIN profile in lenses with larger diameters (Figure 6b) will increase the refractive power and contribute to decreasing the focal length [22].

The spatial and temporal changes we observed in refractive index also correlate with changes in lens protein concentration. A recent protein analysis on zebrafish lenses aged from several days to 27 months post-fertilisation shows that the expression of crystallins, including all three α-, βB3- and γS-crystallins,

increase dramatically between 6 weeks and 4 months post-fertilisation [35]. This corresponds well to the period, up to 120 dpf, in which there is a rapid increase in maximum refractive index and in steepening of the GRIN (Figures 6e and 6f). Refractive index is highest in the lens centre and, as the lens grows, both the magnitude and size of this peak index region increase (Figures 4-6). The peak index values measured in adult zebrafish lenses are around 1.57-1.58, and this is the highest value found amongst all animals measured so far [11, 21, 27, 36, 37] (and reviewed in [5]). The lens protein, γ-crystallin has the highest refractive increment of the lens crystallins [38], and likely contributes more to refractive index than the others. Higher γ-crystallin levels occur in the central lens [39] and is more prevalent in species that have high refractive index values (reviewed in [5]). Aquatic lenses usually have much higher refractive power than those of land animals [22, 40] to compensate for the negligible refractive contribution by the cornea due to the water-cornea interface. Results in the present study show that the GRIN changes with lens growth, particularly the proportions of the central plateau region to the total lens size and the steepness of refractive index in the lens periphery, both critical parameters that contribute to lens focusing power.

The lens grows by continuous accrual of lens fibres cells with no concomitant cell loss resulting in an increase in cells and in their cytoplasmic proteins. This correlates with the rise of peak refractive index (Figure 6a), steepness of the GRIN profile (Figure 6b), protein weight (Figure 6c) and plateau size (Figure 6d). Immunohistochemical analysis reveals that indeed, zebrafish cortical fibre cells, are very flattened (Supp. Figure 1), reminiscent of human cortical lens fibre cells [41]. However, whilst compaction has been cited as a possible cause of refractive index increase [42] and may explain the flattening in the cortical cells (Supp. Figure 1), the nature and force of such compaction has not been properly described. Indeed, recent work in fish lenses shows that fibre cells retain their thickness across the lens in nine piscine species including the zebrafish [43, 44]. Another explanation is that some protein synthesis continues to occur in inner regions of the lens and, given the relatively rapid development and growth of the zebrafish, compared to many larger species, the organelles required for protein synthesis within inner layer cells may still be viable.

Acknowledgements

The authors acknowledge the funding support of beam time grants at SPring-8 synchrotron (grant no 2016A1096, 2017A1197, 2018A1105); Royal Society (grant no IE160996); Zeiss Meditec AG; Fight for Sight UK (1319/1320); National Institutes of Health Grant R01 EY05661.

Author Contributions

B.K. Pierscionek and J.E. Hall initiated this project. I. Vorontsova and J.E. Hall prepared the samples and optical images. K. Wang, M. Hoshino, K. Uesugi, N. Yagi and B.K. Pierscionek conducted the beamtime measurements, K. Wang performed data analysis and prepared the figures with inputs from I. Vorontsova and M. Hoshino. K. Wang and B.K. Pierscionek wrote the first draft of the manuscript, all other authors contributed to the revision of the manuscript.

References

1. Greiling TM, Clark JI. (2012). New insights into the mechanism of lens development using zebra fish. Int Rev Cell Mol Biol. 296, 1-61.
2. Bassnett S, Šikić H. The lens growth process. Prog Retin Eye Res. 2017 Sep; 60: 181–200.
3. Fagerholm PP, Philipson BT, Lindström B. (1981). Normal human lens—the distribution of protein. Exp Eye Res. 33(6), 615-620.
4. Barer R, Joseph S. (1954) Refractometry of living cells. Part 1. Basic Principles. Quart J Microscop Sci. 95, 399–423.
5. Pierscionek BK, Regini JW. (2012). The gradient index lens of the eye: an opto-biological synchrony. Prog Retin Eye Res. 31(4), 332–349.
6. Easter SS Jr, Nicola GN. (1996). The development of vision in the zebrafish (Danio rerio). Dev Biol. 180(2), 646-663.
7. Greiling TM, Clark JI. (2008) The transparent lens and cornea in the mouse and zebra fish eye. Semin Cell Dev Biol. 19(2), 94-99.
8. Westerfield M. (2000). The Zebrafish Book: A Guide for the Laboratory Use of Zebrafish (Danio rerio). 4th ed. (Eugene, OR, University of Oregon Press).
9. Vorontsova I, Hall JE, Schilling TF. (2019). Assessment of Zebrafish Lens Nucleus Localization and Sutural Integrity. J Vis Exp. 147, e59528.
10. Vorontsova I, Gehring I, Hall JE, Schilling TE. (2018). Aqp0a regulates suture stability in the zebrafish lens. Invest Ophthal Vis Sci. 59(7), 2869-2879.
11. Hoshino M, Uesugi K, Yagi N, Mohri S, Regini J, Pierscionek B. (2011). Optical properties of in situ eye lenses measured with X-ray Talbot interferometry: a novel measure of growth processes. PLoS One. 6 (9), e25140.
12. Momose A, Kawamoto S, Koyama I, Hamaishi Y, Takai K, Suzuki Y. (2003). Demonstration of X-ray Talbot interferometry. Jpn J Appl Phys. 42(Part2), L866-L868.
13. Momose A. (2005). Recent advances in X-ray phase imaging. Jpn J Appl Phys. 44(Part1), 6355-6367.
14. Hoshino M, Uesugi K, Yagi N, Mohri S. (2010). Investigation of imaging properties of mouse eyes using X-ray phase contrast tomography. AIP Conf. Proc. 1266, 57-61.
15. Kimmel CB, Ballard WW, Kimmel SR, Ullmann B and Schilling TF. (1995). Stages of embryonic development of the zebrafish. Dev Dyn. 203(3), 253-310.
16. Schilling TF. (2002). The morphology of larval and adult zebrafish. Zebrafish. 261**,** 59-94.
17. Bahrami M, Hoshino M, Pierscionek B, Yagi N, Regini J, Uesugi K.(2014). Optical properties of the lens: An explanation for the zones of discontinuity. Exp Eye Res. 124, 93–99.
18. Collery RF, Veth KN, Dubis AM,Carroll J, Link BA. (2014). Rapid, accurate, and non-invasive measurement of zebrafish axial length and other eye

dimensions using SD-OCT allows longitudinal analysis of myopia and emmetropization. PLoS One. 9(10), e110699.
19. Soules KA, Link BA. (2005). Morphogenesis of the anterior segment in the zebrafish eye. BMC Developmental Biology 5, 1-16.
20. Vihtelic TS, Fadool JM, Gao J, Thornton KA, Hyde DR, Wistow G. (2005). Expressed sequence tag analysis of zebrafish eye tissues for NEIBank. Molecular Vision 11, 1083-1100.
21. Pierscionek B, Bahrami M, Hoshino M, Uesugi K, Regini J, Yagi N. (2015). The eye lens: age-related trends and individual variations in refractive index and shape parameters. Oncotarget. 6(31), 30532-30544.
22. Kröger RH, Campbell MC, Munger R, Fernald RD. (1994). Refractive index distribution and spherical aberration in the crystalline lens of the African Cichlid fish Haplochromis burtoni. Vision Res. 34(14), 1815-1822.
23. Koretz JF, Cook CA, Kuszak JR. (1994). The zones of discontinuity in the human lens: development and distribution with age. Vision Res. 34(22), 2955-2962.
24. Pierscionek BK, Belaidi A, Bruun HH. (2003). Optical development in the foetal bovine lens. Exp Eye Res. 77(5), 639-641.
25. Kröger RH, Campbell MC, Fernald RD. (2001). The development of the crystalline lens is sensitive to visual input in the African cichlid fish, Haplochromis burtoni. Vision Res. 41(5), 549-559.
26. Fernald RD, Wright SE. (1983). Maintenance of optical quality during crystalline lens growth. Nature. 301(5901), 618-620.
27. Birkenfeld J, De Castro A, Ortiz S, Pascual D, Marcos S. (2013) Contribution of the gradient refractive index and shape to the crystalline lens spherical aberration and astigmatism. Vision Res. 86, 27-34.
28. Birkenfeld J, de Castro A, Marcos S. (2014). Contribution of shape and gradient refractive index to the spherical aberration of isolated human lenses. Invest Ophthalmo Vis Sci. 55(4), 2599-2607.
29. Jackson JM, Lenz PH. (2016). Predator-prey interactions in the plankton: larval fish feeding on evasive copepods. Sci Rep. 6, 33585.
30. Verma Y, Rao K, Suresh M, Patel H, Gupta P. (2007). Measurement of gradient refractive index profile of crystalline lens of fish eye in vivo using optical coherence tomography. Appl Phys B. 87(4), 607-610.
31. Garner LF, Smith G, Yao S, Augusteyn RC. (2001). Gradient refractive index of the crystalline lens of the Black Oreo Dory (Allocyttus Niger): comparison of magnetic resonance imaging (MRI) and laser ray-trace methods. Vision Res. 41(8), 973-979.
32. Pierscionek BK, Augusteyn RC. (1995). Refractive index and protein distributions in the blue eye trevally lens. J Am Optom Assoc. 66(12), 739-743.
33. Axelrod D, Lerner D, Sands PJ. (1988). Refractive index within the lens of a goldfish eye determined from the paths of thin laser beams. Vision Res. 28(1), 57-65.
34. Jones CE, Pope JM. (2004). Measuring optical properties of an eye lens using magnetic resonance imaging. Magn Reson Imaging 22(2), 211-220.
35. Wages P, Horwitz J, Ding L, Corbin RW, Posner M. (2013). Changes in zebrafish (*Danio rerio*) lens crystalline content during development. Mol Vis. 19, 408-417.
36. Campbell MC. Measurement of refractive index in an intact crystalline lens. (1984). Vision. Res. 24, 409-415.
37. Pierscionek BK. (1989). Growth and ageing effects on the refractive index in the equatorial plane of the bovine lens. Vision Res. 29(12), 1759-1766.
38. Pierscionek B, Smith G, Augusteyn RC. (1987). The refractive increments of bovine alpha, beta and gamma-crystallins. Vision Res. 27(9), 1539-1541.
39. Vendra VP, Khan I, Chandani S, Muniyandi A, Balasubramanian D. (2016). Gamma crystallins of the human eye lens. Biochim Biophys Acta. 1860(1), 333-343.

40. Jagger WS, Sands PJ. (1996). A wide-angle gradient index optical model of the crystalline lens and eye of the rainbow trout. Vision Res. 36(17), 2623-2639.
41. Lim JC, Walker K L, Sherwin T, Schey KL, Donaldson PJ. (2009). Confocal Microscopy Reveals Zones of Membrane Remodeling in the Outer Cortex of the Human Lens. Invest. Ophthalmol.Vis. Sci. 50 (9), 4304-4310.
42. Sivak, J.G., Dovrat, A. (1983). Aging and the optical quality of the rat crystalline lens. Invest. Ophthalmol. Vis. Sci. 24(9), 1162-1166.
43. Kozłowski, TM, Kröger RH. (2019). Visualisation of adult fish lens fiber cells. Exp Eye Res. 181, 1-4.
44. Kozłowski, TM, Kröger RH. (2019). Constant lens fiber cell thickness in fish suggests crystallin transport to denucleated cells. Vision Res. 162, 29-34.

Figure Legends

Figure 1. **Zebrafish lens orientation for GRIN analysis** Examples of a larval lens (a) and an adult lens (b) *in vivo* illuminated by a transverse external light showing no opacities. Drawings of cross-sectional sagittal plane in larval lens (c) and adult lens (i). Dissected larval lenses (e-h) and adult lenses (j-n) were oriented in sagittal direction (perpendicular to the optical axis) with sutures (found at the anterior and posterior poles of lenses) visible (arrow in d) (d-e, j-k) or imaged from front direction (f-h, l-n). Lenses were imaged by bright field (BF, d, f-g, j, l-m), dark field (DF, e, h, k, n) illumination, or focussed onto a grid place below the lens to assess its ability to focus an image (f, l).

Figure 2. **Parameters characterizing gradient refractive index (GRIN) profiles of zebrafish lenses** (a) GRIN profile plotted against position along the optic axis for a 157 day old lens and (b) GRIN profile of the same lens normalised to the half length of the optic axis and points showing fits to the power exponent model with the value of the power exponent g for the best fit given (c) full GRIN profile of a 157 day old lens, (d) first order derivative of GRIN profile at 157dpf to show over which parts of the profile it shows a plateau and (e) determined plateau region of the GRIN profile.

Figure 3. **Zebrafish lens growth** (a) Zebrafish standard length and (b) lens diameter plotted against age in days post-fertilisation (dpf). The lens diameter peaks and remains around 750 μm after the age of 471dpf.

Figure 4. **2D and 3D refractive index distribution plots** (a-h) Two-dimensional contour plot (left panels) and three-dimensional mesh plot (right panels) of the GRIN profile in the equatorial plane of eight selected lenses aged 15,32,63,66,119,157,471 and 648 days post-fertilisation (dpf) with diameters ranging from 160 to 790 μm. The magnitude of refractive index is colour coded as shown in the colour bar displayed on the right side of each contour plot.

Figure 5. **Fits of normalised GRIN profile to the exponential power model** (a) Nested GRIN profiles for

five selected lenses (b) slopes and exponents g that give best fit to GRIN profiles for each lens showing that with increase in age the slope of the GRIN profile becomes steeper. Normalized lens position is expressed as distance from centre of the lens r over lens radius a. The power exponent g (see Equation 1) depicts the steepness of the GRIN profile.

Figure 6. **Growth of GRIN profile parameters and lens net protein weight with development** (a) Maximum refractive index value plotted against lens diameter, (b) fitted power exponent g plotted against lens diameter, (c) net protein weight plotted against lens diameter, (d) size of central plateau region of each lens plotted against lens diameter, (e) maximum refractive index value plotted against age in dpf and (f) fitted power exponent g plotted versus age in dpf.

Figure 7. **GRIN profiles with age** Nested GRIN profiles of lenses at (a) 15 (b) 32, (c) 63, (d) 66, (e) 119, (f) 471, (g) 648 and (h) 880 dpf showing little variability within age groups.

Supplementary Figure 1. **Zebrafish lens cortical cells**. Adult fixed lens equatorial sections labelled with WGA (red) and DAPI (blue) reveal high level of flattening between the broad sides (A, higher power insert B).

Figure 1

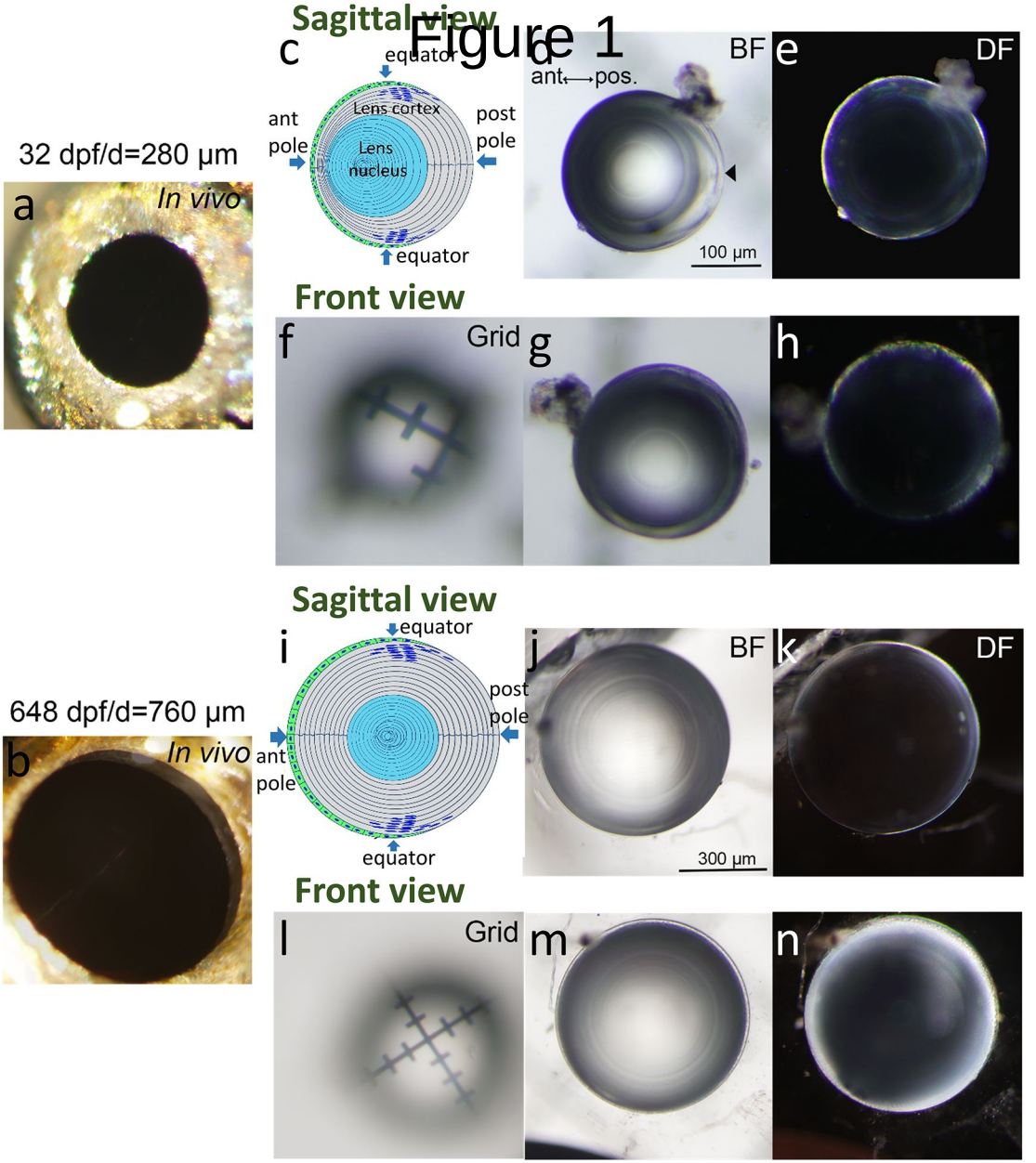
Sagittal view
c
equator
ant pole
Lens cortex
Lens nucleus
post pole
equator
d
BF
ant ⟷ pos.
100 µm
e
DF
32 dpf/d=280 µm
a
In vivo
Front view
f
Grid
g
h
Sagittal view
i
equator
post pole
ant pole
equator
j
BF
300 µm
k
DF
648 dpf/d=760 µm
b
In vivo
Front view
l
Grid
m
n

Figure 2

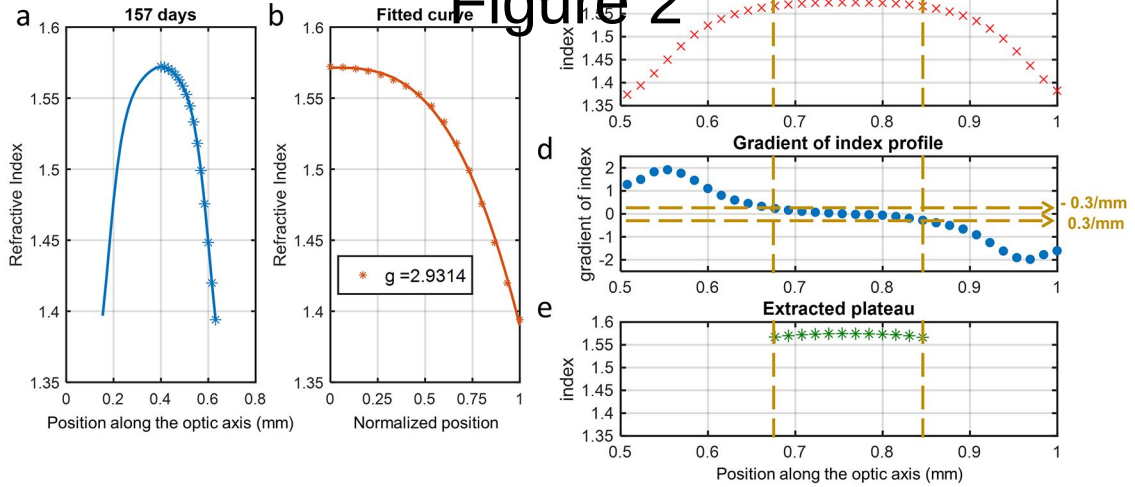
a
157 days
Refractive Index
Position along the optic axis (mm)
b
Fitted curve
g =2.9314
Refractive Index
Normalized position
c
Index profile 157 dpf
index
d
Gradient of index profile
gradient of index
- 0.3/mm
0.3/mm
e
Extracted plateau
index
Position along the optic axis (mm)

Figure 3

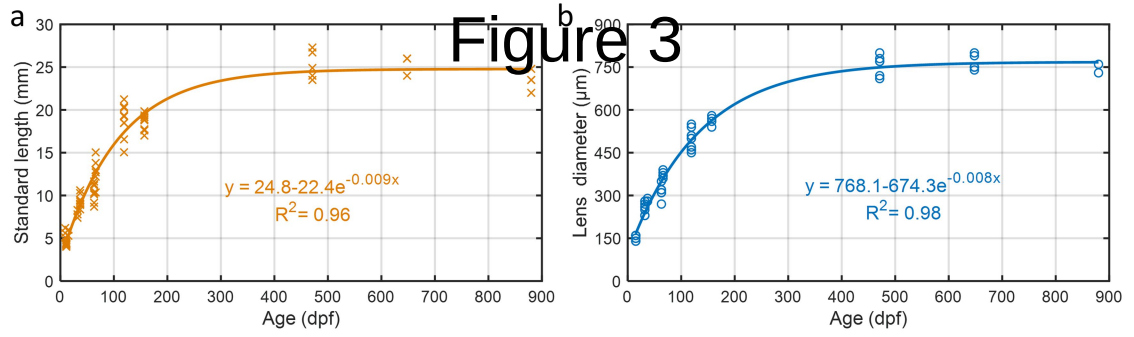
a
Standard length (mm)
Age (dpf)
y = 24.8-22.4e^-0.009x
R^2= 0.96
b
Lens diameter (µm)
Age (dpf)
y = 768.1-674.3e^-0.008x
R^2= 0.98

Figure 4

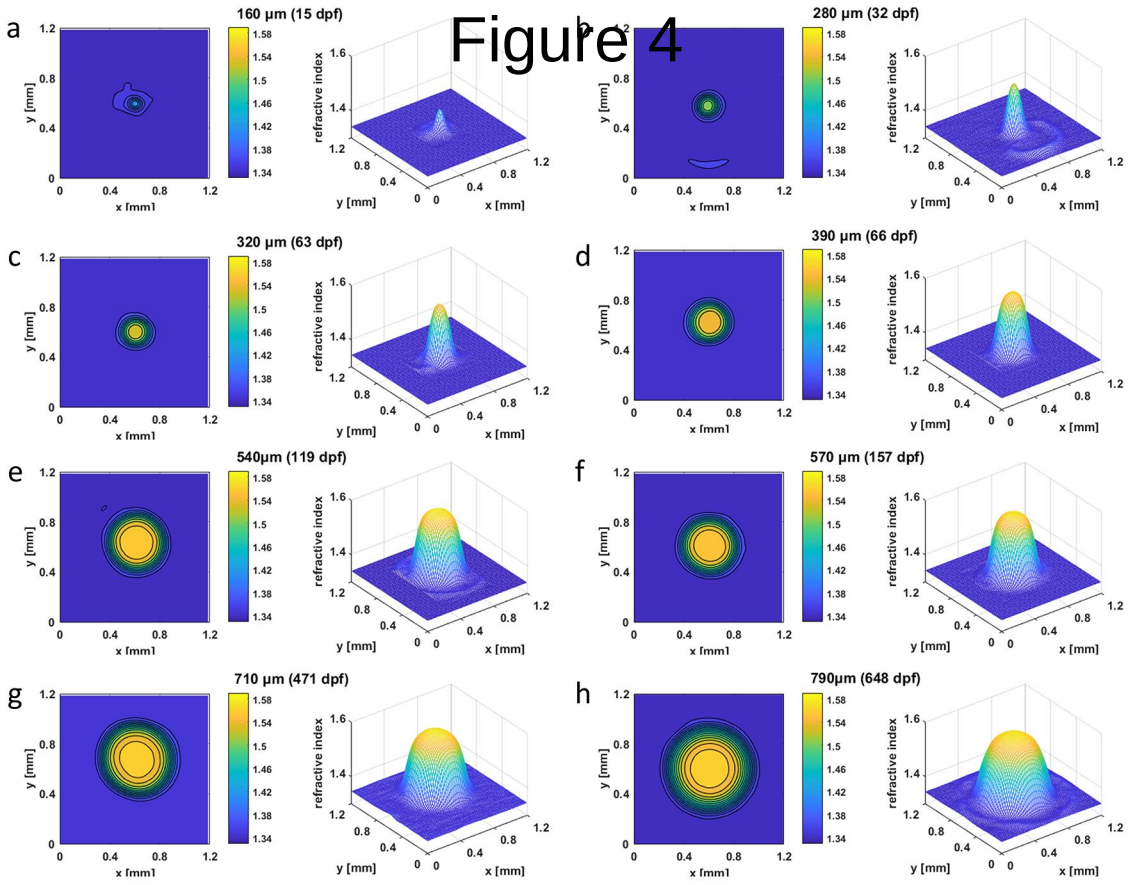
a
160 µm (15 dpf)
b
280 µm (32 dpf)
c
320 µm (63 dpf)
d
390 µm (66 dpf)
e
540µm (119 dpf)
f
570 µm (157 dpf)
g
710 µm (471 dpf)
h
790µm (648 dpf)
y [mm]
x [mm]
refractive index

Figure 5

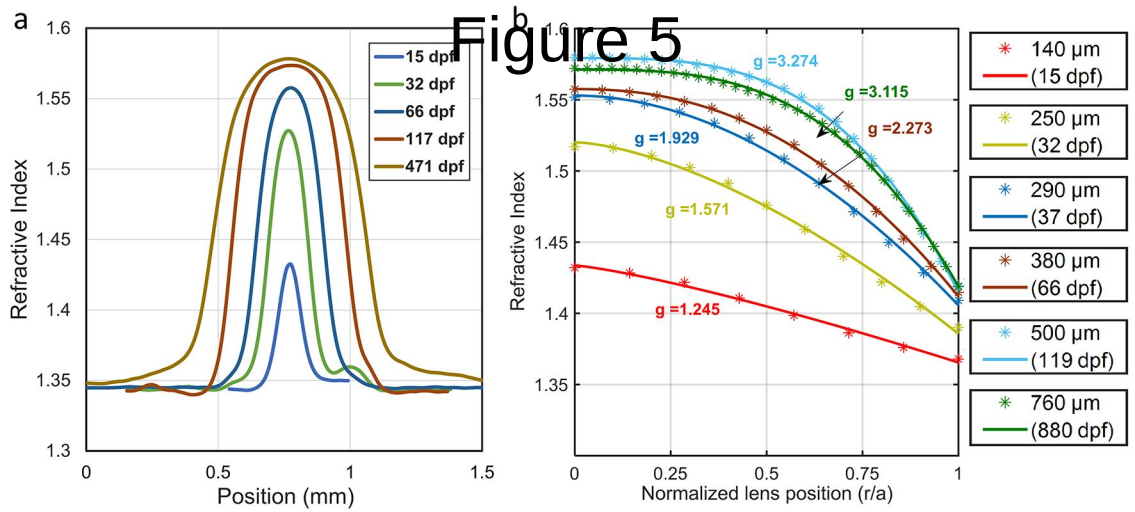
a
b
Refractive Index
Position (mm)
15 dpf
32 dpf
66 dpf
117 dpf
471 dpf
g =3.274
g =3.115
g =2.273
g =1.929
g =1.571
g =1.245
Normalized lens position (r/a)
140 µm
(15 dpf)
250 µm
(32 dpf)
290 µm
(37 dpf)
380 µm
(66 dpf)
500 µm
(119 dpf)
760 µm
(880 dpf)

Figure 6

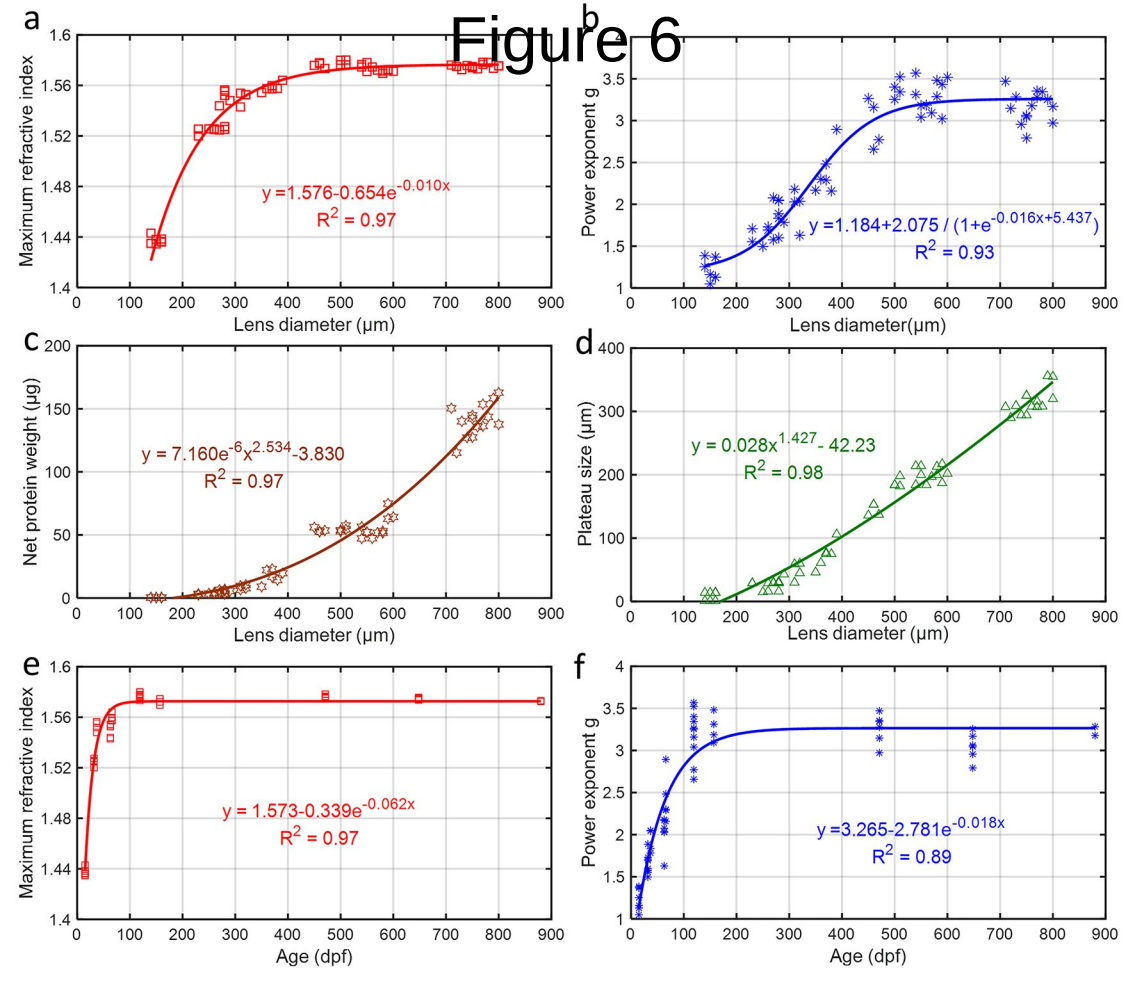
a
Maximum refractive index
y =1.576-0.654e^-0.010x
R^2 = 0.97
Lens diameter (μm)
b
Power exponent g
y =1.184+2.075 / (1+e^-0.016x+5.437)
R^2 = 0.93
Lens diameter(μm)
c
Net protein weight (μg)
y = 7.160e^-6x^2.534-3.830
R^2 = 0.97
Lens diameter (μm)
d
Plateau size (μm)
y = 0.028x^1.427- 42.23
R^2 = 0.98
Lens diameter (μm)
e
Maximum refractive index
y = 1.573-0.339e^-0.062x
R^2 = 0.97
Age (dpf)
f
Power exponent g
y =3.265-2.781e^-0.018x
R^2 = 0.89
Age (dpf)

Figure 7

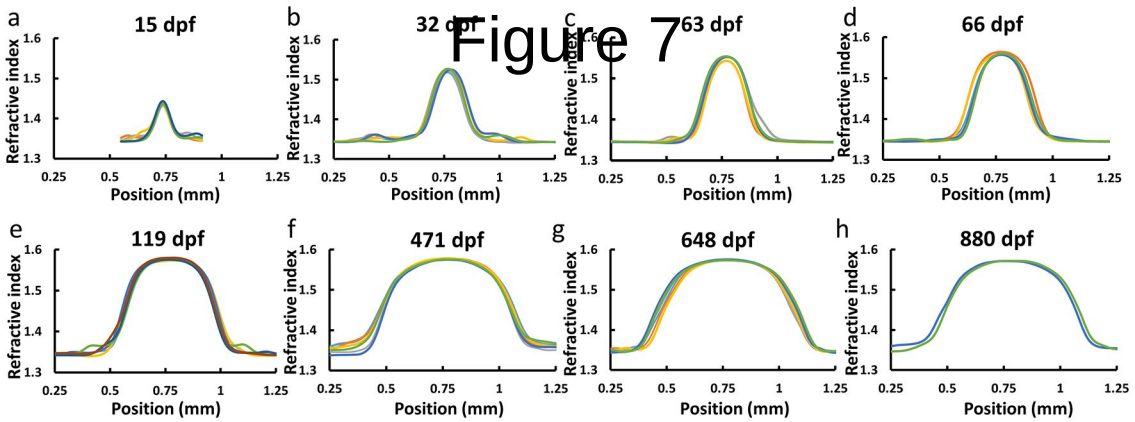
a
15 dpf
b
32 dpf
c
63 dpf
d
66 dpf
e
119 dpf
f
471 dpf
g
648 dpf
h
880 dpf
Refractive index
Position (mm)
1.3
1.4
1.5
1.6
0.25
0.5
0.75
1
1.25

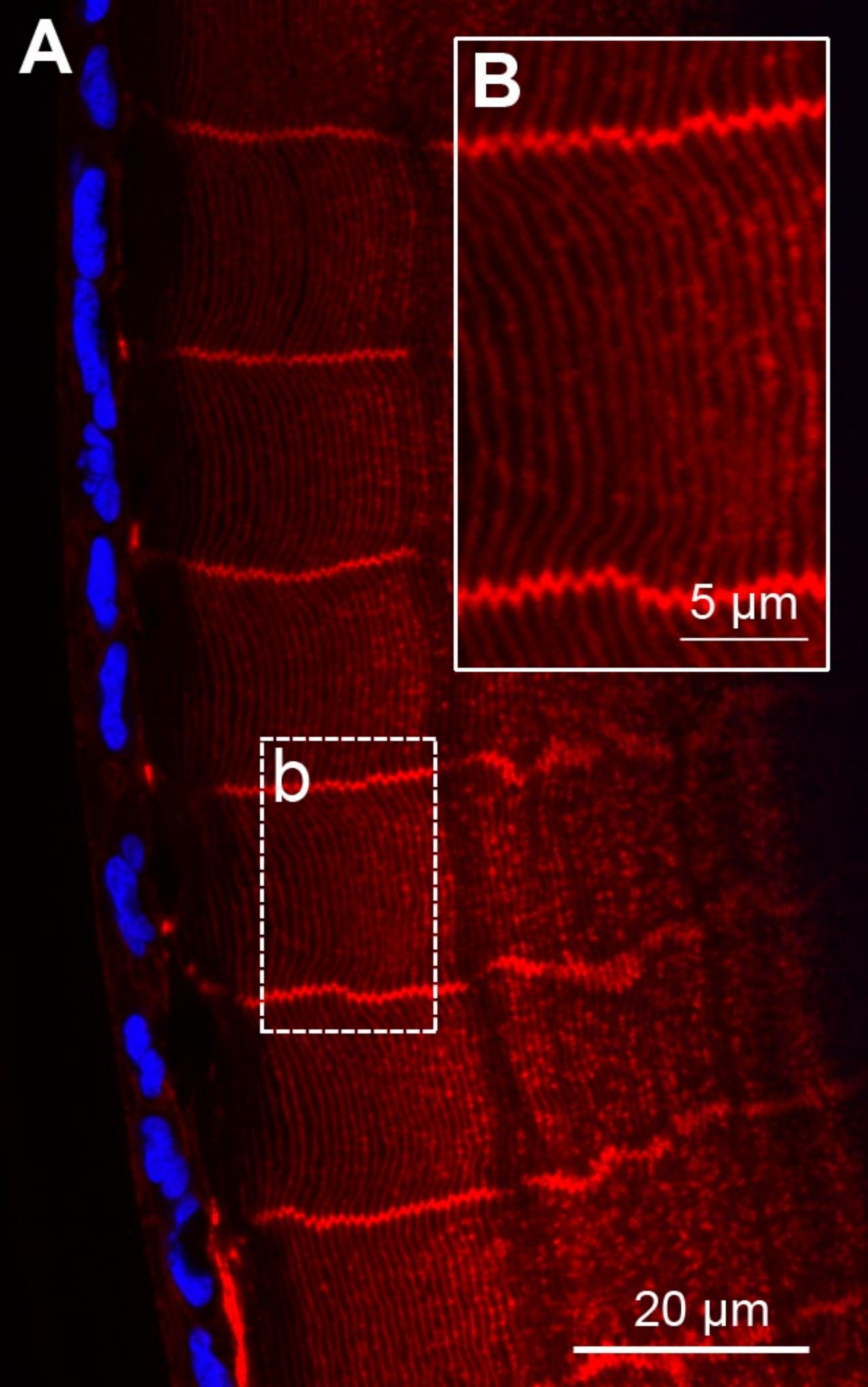
A
B
5 µm
b
20 µm